CrystEngComm

PAPER

View Article Online
View Journal | View Issue

Cite this: *CrystEngComm*, 2016, **18**, 7501

Highly ordered nano-scale structure in nacre of green-lipped mussel *Perna canaliculus*

Sky Shumao Xie,[ab] Oleg Vasylkiv*[ac] and Alfred I. Y. Tok*[b]

The ability of the complex hierarchical structure of nacre to withstand huge work of fracture beyond its constituent materials has generated much interest in its growth mechanism and biomimicry studies. However, the structural features directly involved in the robust mechanical properties have not been successfully identified or emulate in biomimetic materials. In the current article, we present the characterisation of a novel nanostructure framework in nacre of *Perna canaliculus* after chemical etching. The inner structure of the nacre platelet reveals a crystalline three-dimensional framework of orientated fibrous aragonite crystals, which shows that the hierarchical structure at the nano-scale level is much more complex than researchers previously thought. Fracture analysis shows that the fibrous aragonite framework remains largely intact, which indicates the strengthening nature of the elusive internal structure. The discovery of the nano-scale highly ordered structure could be the key to understanding the toughening mechanism in nacre and could serve as a guide to the future biomimetic design of nacre-like, high strength, tough, composite materials.

Received 25th May 2016,
Accepted 23rd August 2016

DOI: 10.1039/c6ce01223j

www.rsc.org/crystengcomm

Introduction

The structured biological material system is a fascinating creation of nature that bestows the abilities of multi-functionality, hierarchical organisation, and adaptability for its own survival.[1] The fundamental requirement for biological materials to assemble into complex hierarchical structures lies in their ability to self-organise from the molecular level up.[2] Furthermore, natural materials can remodel and adapt in response to changing environmental conditions.[3] Nacre, also known as the mother-of-pearl, is a kind of mollusc shell material that has been studied extensively by both biologists and material scientists. Earlier characterisation research on nacre's structure–mechanical properties relationship by Currey[4] and Jackson *et al.*[5] generated much interest with stunning results of 3000-times improvement in the work of fracture as compared to its ceramic constituent and an impressive ability to stop fast travelling cracks owing to the change in material orientation. The biocomposite material has a brick-and-mortar-like structure with up to 95% by volume brittle inorganic polygonal aragonite (a polymorph of calcium carbonate) and a few percent of matrix materials consisting of several types of soft organic biopolymers.

For centuries, researchers have marvelled at nacre's complex hierarchical structure and its abilities to enhance the toughness of the brittle monolithic ceramic material. A unique feature that sets nacre apart from synthetically structured composites is the ability to achieve significant toughening with little or no compromise of strength. Biomimetic nacre-based structured materials have been studied extensively in the research community. Although structured biological materials have appeared to be a viable template in the enhancement of the mechanical properties of brittle ceramics, improvement in toughness without a sacrificial loss in strength is seldom observed. An important feature of structured biological materials that has often been overlooked in biomimetic materials is the complexity of the hierarchical structure ranging from nano-scale up to micro-scale. The hierarchical structure is vital as the structures at different scale levels interact with and complement one another, providing a synergetic improvement of the mechanical properties.[6] Many articles have reported biomimetics of nacre's brick-and-mortar structure;[7–12] however, in most cases only marginal improvements in toughness were achieved and often experienced a sacrificial reduction in strength of the ceramic constituent. Most researchers would agree that the magnitude of enhancement of mechanical properties in nacre is still unrivalled by any man-made ceramic composites and the structure–property behaviour of nacre is still not well-understood.[6,13,14] While one could argue that the low

[a] *Temasek Laboratories, Nanyang Technological University, 50 Nanyang Drive, 637553, Singapore*
[b] *School of Materials Science & Engineering, Nanyang Technological University, Nanyang Avenue, 639798, Singapore. E-mail: miytok@ntu.edu.sg*
[c] *National Institute for Materials Science, 1–2–1 Sengen, Tsukuba, Ibaraki 305–0047, Japan. E-mail: oleg.vasylkiv@nims.go.jp*

enhancement is owing to imperfection in the artificially fabricated brick-and-mortar structure, the author believes that there is still much to be explored within nacre's complex hierarchical structure. The study of the inner structure at the nano-scale level is a vital key to unlocking the mystery behind the huge toughening capability of mollusc shells beyond their constituent materials.

Experimental

Materials and methods

Nacre from the marine mollusc shell of *Perna canaliculus*, also known as green-lipped mussel, was used in the current study. The shell was firstly sawed into equal square plates measuring 5 mm by 5 mm, followed by grinding away of the outer layers using abrasive paper and polishing to reveal the nacreous layer distinguishable by a highly iridescent surface. Multiple samples were prepared from the same *P. canaliculus* mollusc shell for consistency.

A chemical etching approach was used to study the nanostructure of nacre beyond the 'brick-and-mortar' microstructure, which is highly famed for its ability to enhance toughness.[1,2,5,15] The methods of etching nacre have been reported in several papers, some of which include the use of citric acid,[16] EDTA,[17,18] NaOH,[19] HCl,[19] and plasma.[15] Chemical etching of the nacreous layer requires careful preparation of the etchant concentration and control of the etching duration. The samples were etched with different durations from a minimum of 1 minute up to a maximum of 1 hour to study the progression of the etching on the nacre structure. SEM images of non-etched nacre surface were also collected for comparison.

Citric acid ($C_6H_8O_7$) powder from Sigma-Aldrich (ACS reagent, anhydrous, >99.5%) was used to prepare for the chemical etch. The etchant used was freshly prepared for each individual sample by dissolving powdered citric acid with deionised water. The optimal concentration to observe the gradual etch of the nacre structure was found to be around 0.3 moles per litre. Calcium citrate, the product of the reaction, is slightly soluble and can be removed by rinsing with water after the etching process.

Characterisation

SEM and XRD were used extensively in the current research to characterise the hierarchical structure of nacre before and after the etching process. Characterisation of the surface morphology and crystallography were done using a high-resolution field emission scanning electron microscope from JEOL (JSM-7600F, Japan), which can achieve a resolution of up to 1 nm, and X-ray diffraction in reflection mode on a Bruker AXS diffractometer (D8 Advance, Germany) fitted with Cu-tube, CuKα (λ = 0.154 nm), radiation.

Results and discussion

XRD spectra of nacre after being finely ground with an agate mortar and pestle were used to compare the highly orientated aragonite platelets in the nacreous layer with randomly orientated aragonite crystals. X-ray diffraction, as shown in Fig. 1, was used to characterise the nacreous layer of *P. canaliculus*, which consists mainly of aragonite crystals after removal of the outer layers of chitin and calcite.

The nacreous layer of mollusc shells is known to consist of up to 95% aragonite crystals by volume.[5] The XRD profile of the nacreous layer of *P. canaliculus* matches with the crystallographic data (ICDD 00-005-0453) for aragonite crystal. A preferred orientation in the bulk nacre surface was observed where 25 out of the 35 aragonite indexed XRD peaks between the 2θ angle of 20° to 80° were absent in the XRD pattern. With reference to the strongest intensity peak, half of the 10 observed peaks show lower relative intensity, which is a characteristic of oriented crystals. Refinement by Rietveld techniques shows the lattices parameters of a = 4.978 Å, b = 7.980 Å and c = 5.756 Å with a cell volume (V) of 228.691 Å^3 and crystal density of 2.907 g cm^{-3}. An XRD study on an aragonite single crystal by Dickens and Bowen (1971) shows that the lattice parameters and cell volume of a = 4.960 Å; b =7.964 Å; c = 5.738 Å, and V = 226.650 Å^3 are lower than the values in the current study.[20] However, another study by Antao on ammonite shell similarly observed higher values of the lattice parameters and cell volume of a = 4.962 Å, b = 7.970 Å, c = 5.74 Å, and V = 227.222 Å^3 as compared to a single crystal of aragonite.[21] The difference in crystallography between the single crystal and biologically-growth aragonite could be owing to the presence of trace amount of large divalent cations, such as Ba, Sr, and Pb,[20,21] which replace the Ca atoms during the biomineralisation process, thus resulting in higher lattice parameters and cell volume. Nevertheless, the XRD result shows that the nacreous layer of *P. canaliculus* consists

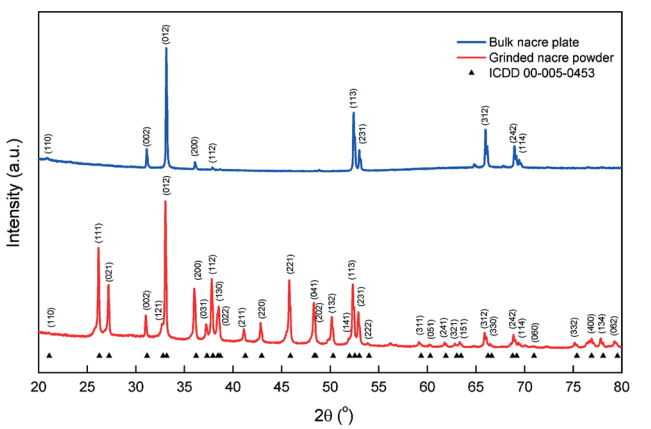

Fig. 1 X-ray diffraction of a bulk nacre plate of *P. canaliculus* nacreous layer (in blue) and fine powder of grinded nacre (in red) shows the strong preferred orientation growth in nacre. Indexed by ICDD 00-005-0453 for aragonite crystals.

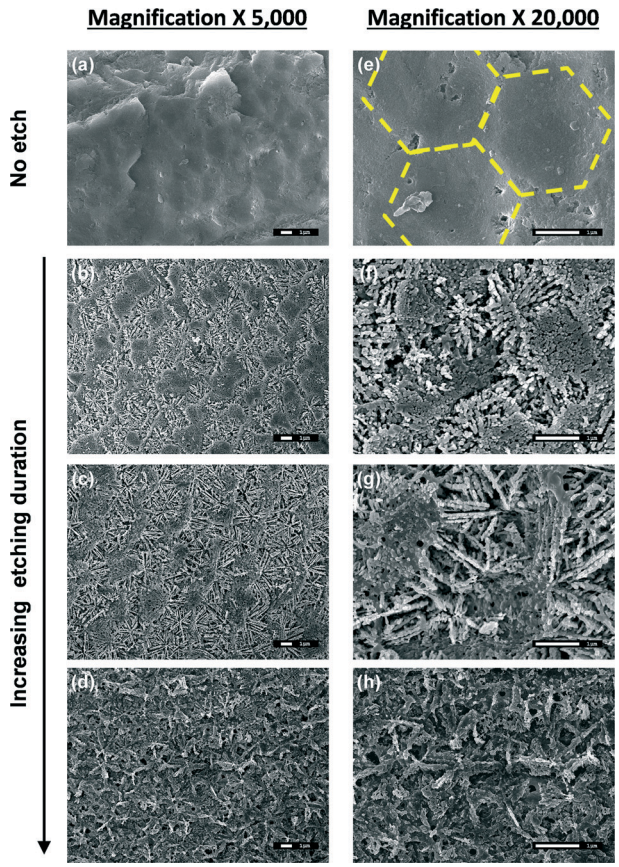

Fig. 2 Progressive etching of *P. canaliculus*'s nacreous layer reveals a remarkable framework of nano-sized particles and fibres arranged in an ordered pattern. (a–d) ×5000 and (e–h) ×20 000 magnification. Hexagonal platelets highlighted in yellow in (e).

largely of orientated crystalline aragonite, which is the focus of the current study.

SEM images of the non-etched *P. canaliculus* nacreous surface are shown in Fig. 2(a) and (e). Individual nacreous platelets can vaguely be seen from the image contrast at the platelet boundary. The hexagonal-shaped platelets are highlighted yellow in Fig. 2(e) for clarity. Each side of the platelet shows an almost perfect hexagonal shape with six equal sides. The width of the platelets was measured to be around 3.2 μm.

The etching process can generally be classified into three different stages. Initial etching of the nacreous layer, as shown in Fig. 2(b) and (f), reveals rows of alternating platelets of different morphologies. The difference in morphology observed is likely owing to the difference in crystal orientation, which affects the etching rate. A study by Hou and Feng[16] on *Mytilus edulis* similarly observed two types of nacre platelet that are characterised by their respective preferred orientation during the growth process. Yao *et al.*,[22] however, observed three distinct orientations on the nacre surface of *Haliotis rufescens*, which indicated that the number of crystallographic orientations on a nacre surface could differ in different mollusc species. In some instances, two or more platelets of the same morphology could be found adjacent to each other. One explanation of such phenomena is the presence of mineral bridges between platelets, which allow growing nacre platelets to take up the orientation of their immediate neighbour during the mineralisation process. Experimental result from Younis *et al.*[23] proved that crystallographic orientations of adjacent nacre platelets connected by the mineral bridges are only slightly tilted to each other, within ±5°. Therefore, the etching rate of the two different types of morphology observed is likely attributed to the two crystallographic orientations in nacre of *P. canaliculus*. Nanoparticles with size ranging from 50 to 100 nm were observed, in agreement with the results obtained by Addadi, Joester, Nudelman and Weiner,[17] typically observed for the mineralisation process from an amorphous precursor.

In the second stage of the etching process, as shown in Fig. 2(c) and (g), nanoparticles of aragonite crystal are subsequently removed to reveal branching fibrous aragonite and a polymeric membrane at the core of each nacre platelet. The polymeric membrane is an aragonite nucleating protein as suggested by earlier research.[24,25] Closer observation of the fibrous aragonite shows a hint of the orderly arrangement that will be explained in detail later in the article. Although both the nanoparticles and fibrous aragonite share the same constituent, $CaCO_3$, the nanoparticles were etched at a slightly faster rate. This is due to the presence of organic inclusion[23] and matrix,[26] consisting of proteins and polysaccharides, which aided in the accelerated removal of the aragonite nanoparticles. On the other hand, solid fibrous aragonite has a slower etching rate, which is shown in the SEM images.

At the last stage of the etching process, as shown in Fig. 2(d) and (h), both the nanoparticles and fibrous minerals are dissolved by the etchant, which is expected as calcium carbonate reacted with citric acid. Some of the fibrous aragonite, however, could still be observed showing the strong resistance to the etchant by the close-packing fibrous aragonite. The discovery of a highly ordered fibrous or needle-like $CaCO_3$ growth in nacre is a significant novel finding. The reason that such complex structured aragonite–aragonite have

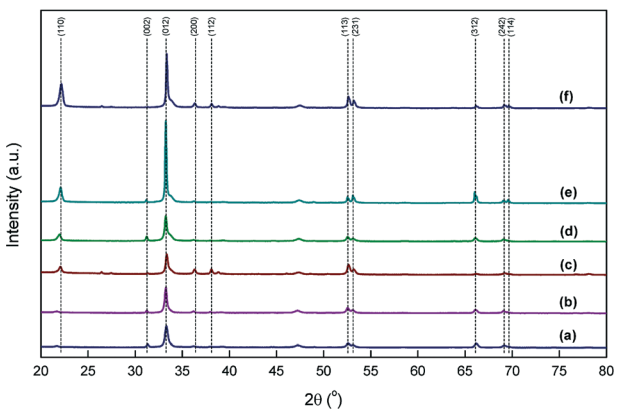

Fig. 3 XRD of *P. canaliculus* nacreous layers non-etched and etched for different durations. (a) Non-etched; (b) 5 minutes; (c) 10 minutes; (d) 20 minutes; (e) 30 minutes; and (f) 40 minutes.

not been observed in any earlier research could be the strong similarity in its constituent material. Another possible reason could be the variation in nacre growth mechanism that is unique to certain species of molluscs.

Fig. 3 shows the XRD of the nacre surface before and after etching for different durations. The chart shows increasing peak intensity, most notably on the (110) and (012) peaks, as the duration of etching lengthens. The increase in crystallinity is indicative of the stripping of the organic inclusions and matrix, revealing the crystalline aragonite within the nacre platelets. Etching beyond 30 min shows a variation in peak intensities, from the rise in the (110) peak and the drop in the (012) peak, indicating a change in the preferred orientation. The XRD matches the SEM observation, indicating the removal of organic components and a change in orientation owing to the appearance of fibrous aragonite.

The nacre growth process is known to be able to form fibrous[26,27] $CaCO_3$ *via* an amorphous $CaCO_3$ precursor. In an earlier work on the study of *Pinna nobilis* mollusc shells by Hovden, Wolf, Holtz, Marin, Muller and Estroff,[26] they describe how the assembly process of fibre-like polycrystalline configuration was driven by aggregation of nanoparticles of size 50 nm to 80 nm within an organic matrix. This coincides with the bamboo-like fibre observed in our SEM images. However, contrary to the 'disordered' needle-like geometry that was described in their article, the fibrous aragonite crystals observed in the current research, as shown in Fig. 4, are highly organised and consistent in shape and size.

Each hexagonal platelet contains six rows of fibres packed in a six-fold rotational symmetry pattern around its core at an angle of 60°. Each row holds a cluster of fibres stacking one over another in parallel with slight misalignment of around ±0.3 μm. The length of each side of the hexagonal shape was measured and estimated to be around 2.0 μm. Earlier research by Mutvei has similarly shown that individual nacre platelets could subdivide into varying amounts of crystalline sectors ranging from 2 to 50;[28] however, no ordered shape and size could be identified, unlike the findings in the current study. This is the first report of such highly ordered and complex arrangement of aragonite crystal in the nacreous layer of *P. canaliculus* mollusc shells to the knowledge of the author.

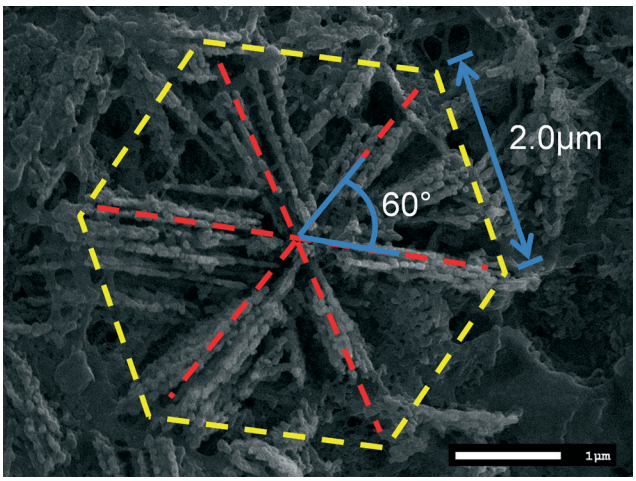

Fig. 4 A single ideally etched platelet revealing the framework of fibrous aragonite crystals with an overlay indicating an angle of 60° between fibre clusters and an estimated length of 2.0 μm for each side of the hexagonal plate.

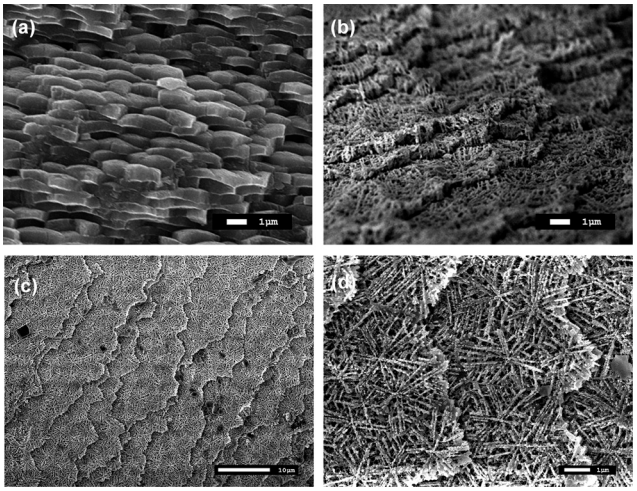

Fig. 5 (a) Cross-section view of the fracture edge of *P. canaliculus*'s nacreous layer. (b) Cross section of the etched fracture edge. (c and d) Top view of the fracture edge showing the nacre fibrous inner structure at magnifications of ×2000 and ×10 000, respectively.

Fig. 5(a) and (b) show the fracture edge of *P. canaliculus* nacreous layer before and after etching. Short vertical fibres could be seen across the thickness of the nacre platelet. The vertical fibres could be the tips of longer stacking fibres, as observed earlier in Fig. 4. Fig. 5(c) and (d) show the top view of the fracture edge at two different magnifications. At low magnification, the outline of each individual platelet can be observed with the jagged edges indicating that the hexagonal shape platelets shape remain largely intact from the fracture. At higher magnification, the fibrous aragonite can be seen arranged in an ordered framework, which could have acted as a reinforcing agent for each individual platelet, preventing the platelet from cracking owing to the impact.

The fibrous nanostructure within the nacre platelets could provide the missing link for the structural hierarchy at the nano-scale level that contributed to the remarkable enhancement of the mechanical properties. Important mechanical property enhancement features that we can observe and learn from the current study are firstly the construct of the hierarchical structure that spans from nano- to micro-scale level allows synergetic dissipation of energy to enhance survivability. Secondly, manipulation of the anisotropic behaviour of the structured material allows maximum protection in a certain direction or area that is most vulnerable to damage. Lastly, structured materials have to achieve long-range ordering and close-packing in order to enable reliable and consistent protection over a selected direction or area of impact.

Conclusions

In conclusion, we have presented the crystallographic analysis of *P. canaliculus* mollusc shell's nacreous layer showing the strong preferred orientation using X-ray diffraction by comparison between a bulk nacre plate and ground nacre powder. Using a chemical etching approach to study the internal structure of nacre platelets, we uncovered a novel highly ordered fibrous aragonite nanostructure framework that has not been reported in any earlier articles. Each nacre hexagonal platelet was found to contain six rows of fibres cluster packed in a six-fold rotational symmetry pattern around its core at an angle of 60° between fibres. Fracture analysis shows that the fibrous aragonite framework remains largely intact, which indicates the strengthening nature of the elusive internal structure. The three-dimensional highly-ordered nanostructure framework in nacre could fill the gap to the understanding of the complex growth mechanism and could serve as a guide to the future biomimetic design of artificial nacre-like, high strength, tough composite materials. We suggest future work to focus on using the current method to examine other species of mollusc shells, the study of the biomineralisation process of fibrous aragonite and the correlation of the material structure–property relationship to better understand fibrous aragonite's role in the enhancement of the mechanical properties of structured composites.

Acknowledgements

This work was supported by funding from Temasek Laboratories @NTU. Material characterisation was carried out at FACTS (Facility for Analysis, Characterisation, Testing and Simulation) in the School of Materials Science and Engineering of Nanyang Technological University.

Notes and references

1 A. V. Srinivasan, G. K. Haritos and F. L. Hedberg, *Appl. Mech. Rev.*, 1991, **44**, 463–482.
2 M. A. Meyers, P. Y. Chen, A. Y. M. Lin and Y. Seki, *Prog. Mater. Sci.*, 2008, **53**, 1–206.
3 M. E. Launey and R. O. Ritchie, *Adv. Mater.*, 2009, **21**, 2103–2110.
4 J. D. Currey, *Proc. R. Soc. London, Ser. B*, 1977, **196**, 443–463.
5 A. P. Jackson, J. F. V. Vincent and R. M. Turner, *Proc. R. Soc. London, Ser. B*, 1988, **234**, 415–440.
6 F. Barthelat, *Philos. Trans. R. Soc., A*, 2007, **365**, 2907–2919.
7 Z. Tang, N. A. Kotov, S. Magonov and B. Ozturk, *Nat. Mater.*, 2003, **2**, 413–418.
8 S. Deville, E. Saiz, R. K. Nalla and A. P. Tomsia, *Science*, 2006, **311**, 515–518.
9 L. J. Bonderer, A. R. Studart and L. J. Gauckler, *Science*, 2008, **319**, 1069–1073.
10 E. Munch, M. E. Launey, D. H. Alsem, E. Saiz, A. P. Tomsia and R. O. Ritchie, *Science*, 2008, **322**, 1516–1520.
11 Z. Burghard, L. Zini, V. Srot, P. Bellina, P. A. v. Aken and J. Bill, *Nano Lett.*, 2009, **9**, 4103–4108.
12 H. Kakisawa, T. Sumitomo, R. Inoue and Y. Kagawa, *Compos. Sci. Technol.*, 2010, **70**, 161–166.
13 J. Xu and G. Zhang, *Mater. Sci. Eng., C*, 2015, **52**, 186–193.
14 D. R. Katti, K. S. Katti, J. M. Sopp and M. Sarikaya, *Comput. Theor. Polym. Sci.*, 2001, **11**, 397–404.
15 R. Z. Wang, Z. Suo, A. G. Evans, N. Yao and I. A. Aksay, *J. Mater. Res.*, 2001, **16**, 2485–2493.
16 W. T. Hou and Q. L. Feng, *J. Cryst. Growth*, 2003, **258**, 402–408.
17 L. Addadi, D. Joester, F. Nudelman and S. Weiner, *Chemistry*, 2006, **12**, 980–987.
18 T. Sumitomo, H. Kakisawa and Y. Kagawa, *J. Struct. Biol.*, 2011, **174**, 31–36.
19 J. Sun and W. Guo, *Sci. China: Phys., Mech. Astron.*, 2010, **53**, 380–388.
20 B. Dickens and J. Bowen, *J. Res. Natl. Bur. Stand., Sect. A*, 1971, **75**, 27–32.
21 S. M. Antao, *RSC Adv.*, 2012, **2**, 526–530.
22 N. Yao, A. K. Epstein, W. W. Liu, F. Sauer and N. Yang, *J. R. Soc., Interface*, 2008, **6**, 367–376.
23 S. Younis, Y. Kauffmann, L. Bloch and E. Zolotoyabko, *Cryst. Growth Des.*, 2012, **12**, 4574–4579.
24 G. Zhang and J. Xu, *J. Struct. Biol.*, 2013, **182**, 36–43.
25 F. Nudelman, B. A. Gotliv, L. Addadi and S. Weiner, *J. Struct. Biol.*, 2006, **153**, 176–187.
26 R. Hovden, S. E. Wolf, M. E. Holtz, F. Marin, D. A. Muller and L. A. Estroff, *Nat. Commun.*, 2015, **6**, 1–7.
27 E. Griesshaber, K. Kelm, A. Sehrbrock, W. Mader, J. Mutterlose, U. Brand and W. W. Schmahl, *Eur. J. Mineral.*, 2009, **21**, 715–723.
28 H. Mutvei, *Zool. Scr.*, 1978, **7**, 287–296.